Extensive flagellar remodeling during the complex life cycle of *Paratrypanosoma*, an early-branching trypanosomatid

Tomáš Skalický[a,b,1,2], Eva Dobáková[a,1], Richard J. Wheeler[c,1], Martina Tesařová[a], Pavel Flegontov[a,d], Dagmar Jirsová[a,3], Jan Votýpka[a,e], Vyacheslav Yurchenko[a,d,f], Francisco J. Ayala[g,4], and Julius Lukeš[a,b,4]

[a]Institute of Parasitology, Biology Centre, Czech Academy of Sciences, 37005 České Budějovice, Czech Republic; [b]Faculty of Science, University of South Bohemia, 37005 České Budějovice, Czech Republic; [c]Sir William Dunn School of Pathology, University of Oxford, Oxford, OX1 3RE, United Kingdom; [d]Life Science Research Centre, Faculty of Science, University of Ostrava, 71000 Ostrava, Czech Republic; [e]Department of Parasitology, Faculty of Science, Charles University, 12844 Prague, Czech Republic; [f]Institute of Environmental Technologies, Faculty of Science, University of Ostrava, 71000 Ostrava, Czech Republic; and [g]Department of Ecology and Evolutionary Biology, University of California, Irvine, CA, 92697

***Paratrypanosoma confusum* is a monoxenous kinetoplastid flagellate that constitutes the most basal branch of the highly diverse parasitic trypanosomatids, which include human pathogens *Trypanosoma* and *Leishmania*. This makes *Paratrypanosoma* uniquely informative for the evolution of obligatory parasitism from free-living lifestyle and the evolution of human parasitism in some trypanosomatid lineages. It has typical promastigote morphology but also forms surface-attached haptomonads and amastigotes. Haptomonads form by attachment to a surface via a large bulge at the base of the flagellum, which is then remodeled into a thin attachment pad associated with flagellum shortening. Promastigotes and haptomonads multiply by binary division, and the progeny of a haptomonad can either remain attached or grow a flagellum and resume swimming. Whole genome sequencing and transcriptome profiling, in combination with analysis of the cell ultrastructure, reveal how the cell surface and metabolism are adapted to parasitism and how characteristic cytoskeletal features are conserved. Our data demonstrate that surface attachment by the flagellum and the flagellar pocket, a *Leishmania*-like flagellum attachment zone, and a *Trypanosoma cruzi*-like cytostome are ancestral features, while evolution of extant trypanosomatids, including the human parasites, is associated with genome streamlining and diversification of membrane proteins.**

trypanosomatid | evolution | flagellar remodeling | haptomonads | cytostome

Kinetoplastid flagellates are diverse and widespread protists, best known for serious human diseases caused by the trypanosomatid genera *Trypanosoma* and *Leishmania*. Most kinetoplastids are successful parasites, infecting a wide range of hosts and with unique and numerous adaptations to the host environment. It is proposed that disease-causing trypanosomatids with two-host (dixenous) life cycles (an insect vector and the mammalian or plant host) evolved from flagellates parasitizing solely insects (1). The earliest known branch of the trypanosomatid clade, predating its diversification, is *Paratrypanosoma confusum*, which infects mosquitoes (2). The free-living clade closest to trypanosomatids is the genus *Bodo* (3, 4).

Emergence of monoflagellated parasitic trypanosomatids from the biflagellated bacteriovorous *Bodo* involved halving of the number of genes (3, 4). To identify further features associated with the evolution of parasitism, we analyzed the morphology of *Paratrypanosoma* and its adaptation to different in vitro environments. Combined with analysis of the genome and transcriptome, this allowed identification of genes potentially associated with these features. The single flagellum of trypanosomatids is a highly flexible structure used for locomotion, attachment, and sensing. Its structure is subject to substantial restructuring during the life cycle to adapt to different functions (5, 6) and is intimately associated with the vital flagellar pocket structure. Flagellar motility is also required

for transmission, immune evasion, and cell division (7) of *Trypanosoma brucei*. Recently further flagellar functions, including production of extracellular vesicles that may mediate host interaction (8) and parasite–parasite interaction by membrane exchange or fusion (9), have been described. In the juxtaform morphological superclass (trypo- and epimastigotes), the flagellum is laterally attached to the cell by an extended flagellum attachment zone (FAZ). Alternatively, in the liberform morphological superclass, the flagellum may protrude from the flagellar pocket without an extended attachment (pro-, opistho-, and choanomastigotes) (10).

Here we report that *Paratrypanosoma* and stercorarian trypanosomes, including *Trypanosoma cruzi* and *Trypanosoma grayi*, retain more ancestral genes than other trypanosomatid clades. Despite having liberform morphology, *Paratrypanosoma* has flagellum–cell attachment via a small FAZ in the flagellar pocket similar to *Leishmania* (11). It also has a complex cytostome architecture similar to *T. cruzi* (12) but lost in *T. brucei* and *Leishmania*

Significance

Kinetoplastids are a group of protists with unique morphology and molecular features. Many have developed a parasitic lifestyle and are economically and medically important causative agents of serious crop, animal, and human diseases. Evolutionarily, *Paratrypanosoma confusum* sits between parasitic trypanosomatids and free-living bodonids and therefore is uniquely informative for study of the emergence of parasitism. It is morphologically very flexible, as it forms three distinct life stages that can be studied separately. Particularly interesting is the haptomonad stage in which it rebuilds its flagellum into an extensive adhesive plaque. As an adaptation to parasitism, *Paratrypanosoma* lost a plethora of enzymes involved in breakdown of macromolecules and the capacity of receptor-mediated endocytosis but has gained surface proteins and membrane transporters to obtain nutrients from the host.

MEDICAL SCIENCES

Fig. 1. Morphologies of *Paratrypanosoma*. (*A*) Different morphologies by light microscopy of Giemsa-stained cells (*Left*) and SEM (*Right*). Promastigotes have a long flagellum with a prominent bulge at its base (*Inset*). The kineto-plast (K) and nucleus (N) are indicated. Neither haptomonads nor amastigotes have a long flagellum. (*B*–*E*) SEM of haptomonads. (*B*) Haptomonads attach perpendicular to the surface in dense clusters. (*C*) Haptomonad cluster de-tached from the surface by propylene oxide showing the underside of the attachment pad. (*D*) Haptomonads retain a bulge at the tip of their short flagellum. (*E*) Occasional long flagella are visible extending from the hapto-monad attachment pad. [Scale bars: 5 μm (*A*, *B*, and *C*; except in *A*, *Middle* image, 10 μm, and *Inset*, 1 μm), 1 μm (*D*), and 2 μm (*E*).]

mexicana. Furthermore, it is able to restructure the flagellum to attach to surfaces, generating an extensive flagellum-derived ad-hesive pad, and does so readily in culture. This allowed an analysis of this process, which occurs in most trypanosomatid lineages (13–15). Judging by the distribution of morphological traits in trypa-nosomatids, we propose that *Paratrypanosoma* morphology is close to that of the last common ancestor of trypanosomatids.

Results

The discovery of *Paratrypanosoma* as an outgroup to all other trypanosomatids calls for a study focused on the distribution of morphological and molecular traits on the trypanosomatid tree. Light microscopy of live and Giemsa-stained cells and scanning electron microscopy (SEM) showed that in liquid medium axenic *Paratrypanosoma* attains both a motile promastigote with a long free flagellum (Fig. 1*A*) and a sedentary, surface-attached stage similar to haptomonads of *Leishmania* (16). The haptomonad stage

formed extensive thin attachment plaques on plastic substrates (Fig. 1 *B*–*E*). We have also observed these morphologies in the gut of the *Culex quinquefasciatus* host. On semisolid agar, *Para-trypanosoma* attained a third morphology: an amastigote without a noticeable free flagellum (Fig. 1*A*). These morphologies are typical of monoxenous trypanosomatids: haptomonads during surface at-tachment in the gut of the invertebrate host, and amastigotes when excreted. All *Paratrypanosoma* morphologies lack an extended FAZ, typical of the liberform morphological superclass (11).

We have been unable to ascertain the relation of axenic culture cell morphologies to the *Paratrypanosoma* life cycle, which is not well understood. In *C. quinquefasciatus* mosquitoes infected either by feeding on sugar or blood meal, *Paratrypanosoma* was detected in the gut and/or crop on the first (100% specimens, $n = 8$), second (100%, $n = 9$), and third day postinfection (90%, $n = 10$) but not after defecation. Gaining and retention of the infection from third or fourth instar larvae through pupation to adult mosquitos were tested by addition of promastigotes into water containing the larvae, where the promastigotes survive for at least 2 d. The adult mosqui-toes of both sexes were never infected ($n = 80$). This may suggest defective infectivity of the culture-adapted parasites. *Paratrypanosoma* fail to survive at 37 °C for more than a few hours, suggesting a monoxenous lifestyle. We also attempted to infect four BALB/c mice by a combination of s.c. and i.p. injection of 10^7 promastigotes, however 1–4 wk postinfection parasites were detected neither by cultivation nor PCR. Nonetheless, life cycles with the promastigote, surface-attached haptomonad, and amastigote stages are common among insect-parasitizing trypanosomatids (11), and promastigotes and haptomonads occur in *Leishmania* vectors (16), making analysis of *Paratrypanosoma* morphology and ultrastructure in vitro valuable.

Surface attachment is widespread among trypanosomatids, yet the development of the plaque used for attachment (Fig. 1 *B*–*E*) has not been studied in detail. Therefore, we analyzed transition of *Paratrypanosoma* between the promastigote and haptomonad morphologies by time-lapse light microscopy in culture (Fig. 2) with reference to the morphology of haptomonads by SEM (Fig. 1 *B*–*E*). Surface attachment of promastigotes occurred by the base of the external flagellum: the "bulge" (Fig. 1 *A* and *D*). Following attachment, the flagellum shortened until it barely extended from the flagellar pocket, taking around 1 h (Fig. 2 and Fig. S1*A*). This was associated with the cell repositioning to an upright orientation and the bulge spreading into a thin extended pad attached to the surface. A colony of haptomonads could

Fig. 2. Promastigote attachment and replication as a haptomonad. Shown are frames from time-lapse videos of promastigote and haptomonad interconversion. Attachment of a promastigote to form a haptomonad and two successive divi-sions, first forming two haptomonads and then two haptomonads and two promastigotes. Time (hours:minutes) for each frame is shown in the top right, and a cartoon of cell arrangement is shown in the bottom left. (Magnification: 100×.)

cover a large area by these extended pads. Time-lapse light microscopy indicated haptomonads can divide while attached, generating daughter cells that may remain attached or grow an extended flagellum and detach (Fig. 2 and Fig. S1*B* and Movies S1 and S2). The cell cycle took ∼6 h at 20 °C, while elongation of the flagellum and detachment took 1–2 h (Fig. 2).

Transformation from promastigotes into haptomonads was promoted by nutrient availability and alkaline pH. The digestive tract of a mosquito is nutrient-rich and typically alkaline (17) and is thus suitable for haptomonads. The attachment pad was highly resistant to our attempts to degrade it enzymatically (Dataset S1), indicating it could confer strong attachment even under harsh digestive conditions in the mosquito gut. Formation of haptomonads, like life cycle transitions in other species, includes significant remodeling of the flagellum. We therefore sequenced the *Paratrypanosoma* genome for analysis of evolution of the flagellum and flagellum-related cytoskeleton and as a reference for transcriptome analysis of different morphological stages for insight into metabolism.

Using paired-end and mate-pair Illumina reads, we assembled a 31.4 Mbp draft genome with 31× average coverage and 2,114 scaffolds (maximum length, 2.99 Mbp; N50 of 438 Kbp). Using Augustus trained on a set of unambiguous gene models for conserved genes and RNA-sequencing (RNA-seq) read mapping, we annotated 8,668 protein-coding genes, 66 tRNAs, and 122 rRNA genes. This gene complement is comparable to other trypanosomatids (18). Most core eukaryotic genes (72.3%) were present [a similar proportion to high-quality *T. brucei* (74.9%), *Leishmania major* (73.6%), and *Leptomonas pyrrhocoris* (72.6%) genomes], indicating a complete genome assembly (19). RNA-seq comparison of gene expression between haptomonads and promastigotes revealed 327 and 264 genes significantly up-regulated, respectively (false discovery rate corrected *P* value < 0.05, fold-change > 2) (Dataset S2). The most up-regulated genes in haptomonads were associated with the ribosome or translation (Dataset S3*A*), while those up-regulated in promastigotes were mostly part of intermediary metabolism or redox processes (Dataset S3*B*).

We used comparative genomics to investigate whether *Paratrypanosoma* has retained more ancestral features than other trypanosomatids. Using OrthoFinder (20), we defined orthologous groups (OGs) of proteins for a large set of trypanosomatids, three bodonids (free-living *Bodo saltans* and *Neobodo designis*, and parasitic *Trypanoplasma borreli*), endosymbiotic *Perkinsela* sp., and *Naegleria gruberi*, a heterolobosean (Fig. 3 and Dataset S4). Next, we counted the number of ancestral OGs (OGs shared with any bodonid or *Naegleria*). *T. grayi*, a stercorarian trypanosome crocodile parasite, had the highest number of ancestral OGs (6,197), while *Paratrypanosoma* had the second highest (6,066). This was as expected given that both species have the shortest branches in a multigene tree (Fig. 3). Therefore, these two species are the slowest evolving trypanosomatids in our dataset.

We also scrutinized the distribution of ancestral OGs across major mono- or paraphyletic groups: (*i*) *Paratrypanosoma*, (*ii*) salivarian and (*iii*) stercorarian trypanosomes, (*iv*) Leishmaniinae (*Leishmania*, *Leptomonas*, *Crithidia*), (*v*) *Phytomonas*/*Blechomonas*, and (*vi*) bodonids/*Perkinsela*/*Naegleria*. Stercorarian trypanosomes and *Paratrypanosoma* had the highest numbers of ancestral OGs unique to those clades: 123 and 112, respectively. When ancestral OGs occurring in any two trypanosomatid clades were considered, *Paratrypanosoma* and stercorarian trypanosomes coinherit by far the highest number of OGs (235), while other intersections contained 54 OGs or less (Fig. 3). Most *Paratrypanosoma* genes with these phyletic patterns were hypothetical proteins or lacked specific annotation (Datasets S5 and S6), however we observed (*i*) some genes of tryptophan and histidine catabolism and arginine biosynthesis are unique to *Paratrypanosoma* and/or stercorarian trypanosomes and were lost in the other trypanosomatids and (*ii*) proteins of the dispersed gene family 1 (DGF1) (21) are
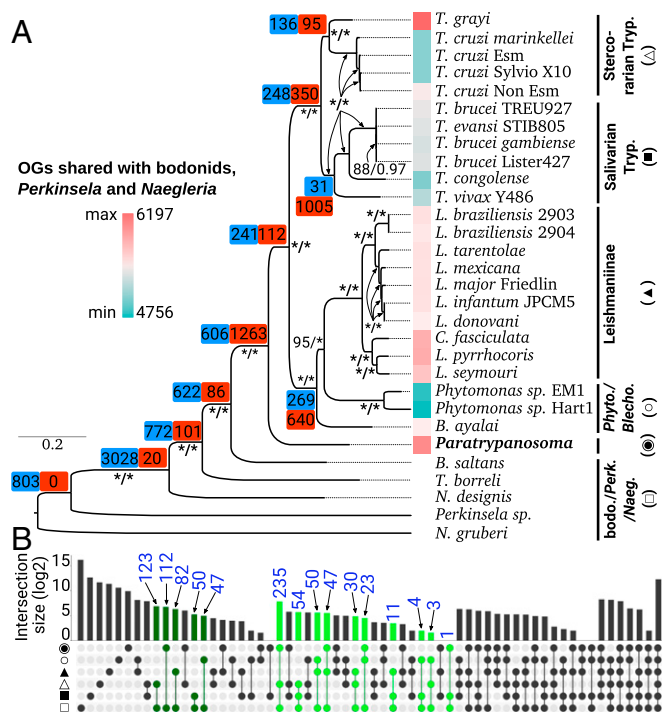

Fig. 3. Ancestral gene families in *Paratrypanosoma* and other trypanosomatids. (*A*) Trypanosomatid phylogenetic tree based on 98 contatenated protein sequences. Tree node support is shown as "bootstrap support/posterior probability," and "*/*" indicates full support. Counts of OGs shared with one bodonid and/or *Naegleria* are color-coded per species (scale on left). OG gains (blue) and losses (red) were mapped by Dollo parsimony. Fewer basal nodes are shown for clarity (Fig. S6). (*B*) Phyletic patterns visualized for six clades: filled circle, *Paratrypanosoma*, ○ *Phytomonas/Blechomonas*; filled triangle, *Leishmania/ Leptomonas/Crithidia*; open triangle, stercorarian trypanosomes, filled square, salivarian trypanosomes; open square, bodonids/*Perkinsela/Naegleria*. Counts of OGs unique to each clade and all possible intersections of the six clades are shown, plotted on a log scale with selected counts indicated. Counts of ancestral OGs shared by one (dark green) or two (light green) clades are indicated.

unique to *Paratrypanosoma* and stercorarian trypanosomes. This is remarkable, as DGFs are the fifth largest protein family in *T. cruzi*. They are long membrane proteins of unknown function stored in intracellular vesicles, with their extracellular domains secreted during transformation to the amastigote (21, 22). The DGF1 proteins are up-regulated in the *T. cruzi* amastigote relative to the trypomastigote and epimastigote (21), while in *Paratrypanosoma* they tended to be up-regulated in the haptomonad (Dataset S2).

Finally, we looked at the relationship of phyletic patterns and functional categories for OGs. Using a one-way ANOVA with Tukey's honest significance test, we saw that differential gene expression in the haptomonad and promastigote stages depended on phyletic patterns of corresponding OGs (*P* value = 1.22×10^{-7}; Dataset S7). Ancestral genes inherited only by stercorarian trypanosomes and *Paratrypanosoma* tended to be up-regulated in haptomonads: 84 genes in this group had significant changes in their expression, of which 55 were up-regulated in haptomonads and 29 in promastigotes (Dataset S2). Stage-specific expression of this group was significantly different to universally conserved genes, genes shared by *Paratrypanosoma* and both *Trypanosoma* clades only (but not bodonids), and *Paratrypanosoma*-specific genes (*P* values adjusted for multiple testing = 0.012, 0.006, and 8×10^{-7}, respectively). Genes within the two latter groups tended to be up-regulated in promastigotes. Overall, ancestral genes were typically constitutively expressed in *Paratrypanosoma* or up-regulated in haptomonads, while trypanosomatid-specific genes tended to be up-regulated in the promastigote (Dataset S7). This

suggests that the haptomonad stage might be an ancestral characteristic of trypanosomatids.

The dramatic morphological change between promastigotes and haptomonads is formation of the adhesive pad from the bulge at the base of the promastigote flagellum. As this may involve restructuring of the paraflagellar rod (PFR), FAZ, and flagellar axoneme, we analyzed conservation across kinetoplastids of proteins known to form these structures (Fig. S2). The FAZ proteins are of particular interest as they have adaptable functions in cell morphogenesis. They were first identified in the extended FAZ of *Trypanosoma* but are also components of the flagellar pocket neck in *Leishmania* promastigotes (11).

Using TEM and electron tomography, we analyzed the structure of the pocket and base of the flagellum to determine the ultra-structural features responsible for the haptomonad morphological adaptation. TEM revealed extensive attachment of the bulge to the cell body by desmosome-like structures in promastigotes and haptomonads, comparable to the *Leishmania* flagellar pocket neck, albeit covering a larger area (Fig. S3 *A* and *B*). This suggests the proteins involved in bulge-cell attachment are the FAZ proteins, and RNA-seq showed FAZ mRNAs were present in both promastigotes and haptomonads. Attachment is particularly complex in the distal pocket region, likely mediated by FAZ10, and this attachment was elaborated in haptomonads (Fig. S3*B*). Immunofluorescence using the anti-*T. brucei* FAZ antibody Dot1 identified a structure in promastigotes near the expected localization of FAZ10, which also showed elaboration in haptomonads (Fig. S3*C*). The *Paratrypanosoma* genome encodes orthologs of almost all FAZ proteins (Fig. S2*A*), while *Bodo* and *Neobodo* have orthologs of around half. The trypanosomatids therefore appear to have diversified FAZ proteins. Given the ancestral trypanosomatid was likely liberform, we propose that the FAZ proteins originally evolved to generate the haptomonad morphotype. The extended FAZ of the juxtaform *Trypanosoma* later arose in that lineage. Some FAZ proteins are often lost among liberforms (FAZ4, FAZ13), and some OGs (FLA, FLABP, FAZ11) show duplication among juxtaforms. Further candidates for forming the extended FAZ may be identified among OGs gained at the *Trypanosoma* node (Datasets S5 and S8).

SEM of promastigotes revealed a cytostome-like indentation near the cell anterior (Fig. 1*A* and Fig. S4*A*). TEM of the pocket structure (Fig. S4*B*) and 3D reconstruction of the pocket organization by electron tomography showed that overall the pocket was typical of promastigotes, including those of *Leishmania*, with a simple invagination surrounded by complex electron-dense areas and sets of microtubules (Fig. 4). There were two sets of specialized microtubules: a quartet similar to the FAZ quartet of *T. brucei* and *Leishmania* (23), and a highly decorated set of microtubules associated with the cytostome. These ran from the pocket neck around the preoral ridge, back to a dip in the cell surface from which microtubules extend into the cytoplasm (Fig. 4 and Fig. S4*A*). This structure is comparable to the *T. cruzi* cytostome/cytopharynx (11). This suggests the *Leishmania*-like flagellar pocket neck/FAZ structure and microtubule quartet were ancestral and later extended into the long *Trypanosoma* FAZ. It also indicates the cytostome was present in the ancestral trypanosomatid; has been lost in *Leishmania*, many monoxenous trypanosomatids, and salivarian trypanosome lineages; but retained in stercorarian trypanosomes, some monoxenous parasites (including *Crithidia fasciculata*), and *B. saltans* (24). No gains or losses of FAZ OGs suggested a function in formation of the cytostome.

The *Paratrypanosoma* promastigote flagellum has the canonical 9+2 axoneme and, based on the genome sequence, a canonical molecular composition (Fig. S2). Both haptomonads and amastigotes have greatly shortened flagella. In *Leishmania*, flagellar shortening during transition to the amastigote is associated with loss of the central pair, distal motor proteins, and radial spokes, giving a transition from a 9+0 to a collapsed 9v (variable)
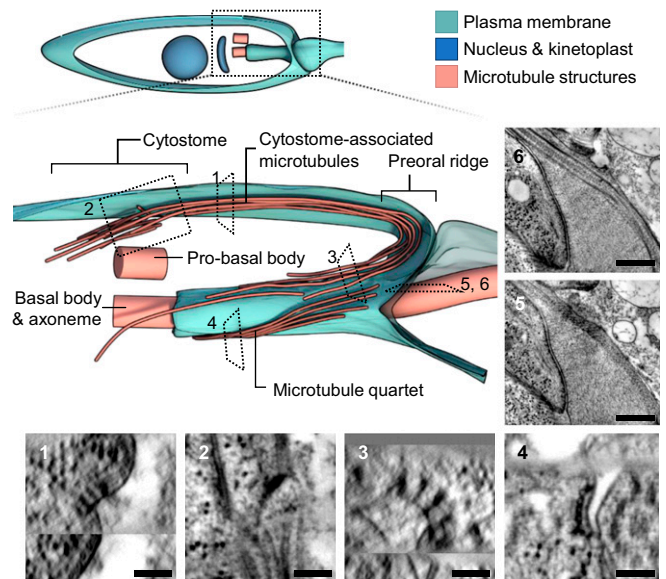

Fig. 4. *Paratrypanosoma* has a cytostome similar to *T. cruzi* and a pocket architecture similar to Leishmania. 3D model of the pocket/cytostome of *Paratrypanosoma* assembled from an electron tomogram, with the approximate position of the tomographic volume within a promastigote cell indicated. Virtual sections through the preoral ridge (*1*), the cytostome (*2*), the cytostome microtubules exiting the pocket (*3*) and the FAZ-associated microtubule quartet (*4*), the PFR (*5*), and axoneme next to the PFR (*6*) are shown. The quasi-crystalline structure of the PFR (*5*) was only present immediately next to the axoneme (*6*) in the promastigote bulge. (Scale bars, 100 nm.)

axoneme (6). We used TEM to check whether similar axoneme restructuring occurred in *Paratrypanosoma* (Fig. 5). Longitudinal sections through the promastigote, haptomonad, and amastigote flagellum base showed a basal plate and central pair, while longitudinal sections and Markham rotational averaging showed a presence of the central pair, radial spokes, and inner and outer dynein arms in all three stages (Fig. S5). RNA-seq data confirmed this result, with central pair, radial spoke, and dynein arm light and intermediate chains not significantly regulated between promastigotes and haptomonads (Dataset S9). Essentially all axonemal components were conserved in all species analyzed (except *Perkinsela*, which has lost its flagellum), providing no putative markers for the 9v axoneme formation.

The PFR is normally present in trypanosomatid flagella but is usually lost in amastigotes. We therefore asked if the PFR is present in different developmental stages and whether it restructures to form the haptomonad adhesive pad. TEM showed the PFR is present in promastigotes but was shortened or absent in haptomonads and amastigotes (Fig. 5 *A*–*C*). Immunofluorescence using an antibody recognizing PFR2, a major PFR component, showed a similar PFR in promastigotes to *Trypanosoma* and *Leishmania* and uneven loss of the PFR in haptomonads (Fig. 5*D*). The characteristic quasi-crystalline structure of the PFR was only visible immediately next to the axoneme in the promastigote bulge and haptomonad attachment plaque (Fig. 4), suggesting that elaboration of the flagellum does not involve expansion of the PFR. RNA-seq also showed similar PFR mRNA levels between promastigotes and haptomonads (Dataset S9). Comparative genomics revealed that *Bodo* and *Paratrypanosoma* possess almost all known PFR components, indicating greater conservation of the PFR than the FAZ.

Promastigote to haptomonad interconversion was modulated by the growth medium, suggesting links between morphological adaptation and metabolism. We analyzed which metabolic pathways are likely active in *Paratrypanosoma* and which were lost early in
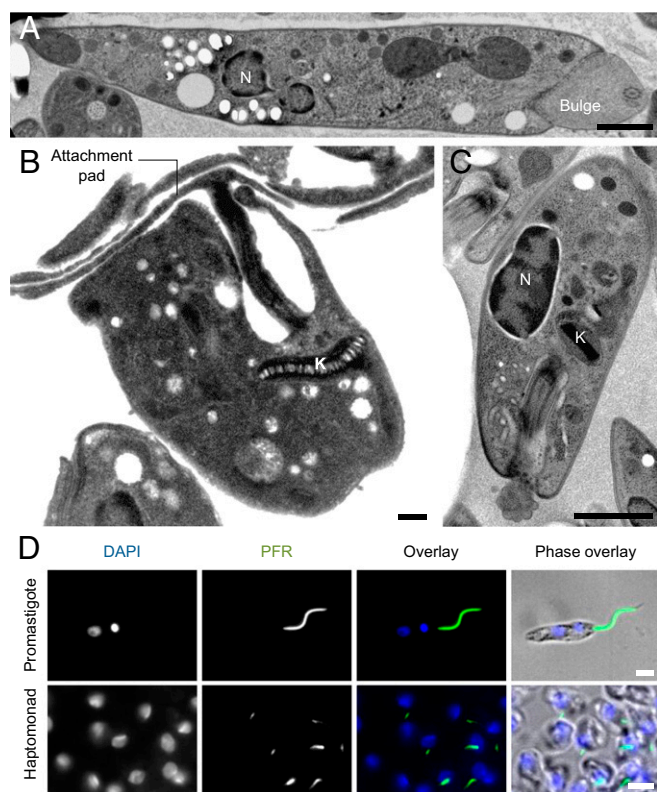
Skalický et al.

Fig. 5. Restructuring of the *Paratrypanosoma* flagellum between promastigotes, haptomonads, and amastigotes. (*A*–*C*) TEM showing the morphology of the flagellum in (*A*) promastigote, (*B*) haptomonad, and (*C*) amastigote. The attachment pad in haptomonad is continuous with the flagellum. (*D*) Immunofluorescence of promastigotes and haptomonads using an anti-PFR antibody. The PFR is reduced or absent in haptomonads. [Scale bars, 1 μm (*A* and *C*), 250 nm (*B*), and 2 μm (*D*).] K, kinetoplast; N, nucleus.

the evolution of trypanosomatids (Dataset S10). In comparison with *B. saltans*, *Paratrypanosoma* has lost many proteases, peptidases, cathepsins, and enzymes for hydrolysis of complex sugars. This suggests a loss of enzymes for digestion of complex energy sources early in the evolution of parasitism. With the exception of xanthine–guanine phosphoribosyltransferase, *Paratrypanosoma* encodes all components of the purine salvage pathway, which is thus likely operational (Dataset S10). However, it lacks arginases needed for the urea cycle and has lost ornithine aminotransferases and xanthine dehydrogenases and therefore may indicate the urea cycle and oxidative metabolism of purines are not possible (Dataset S10). Concerning lipid metabolism, it possesses the methylmalonyl pathway, which converts propionyl-CoA, a product of odd chain fatty acid oxidization, into succinyl-CoA. This pathway has been lost in salivarian trypanosomes and *Phytomonas* (Dataset S10). *Paratrypanosoma* has all of the enzymes needed for ether–lipid biosynthesis except 1-acyl-sn-glycerol-3-phosphate acyltransferase, which may indicate an inability to perform the second acyltransferase reaction of phosphatidic acid formation. It also encodes a pathway needed for phosphonolipid formation carried out by phosphoenolpyruvate mutase, previously identified only in *B. saltans* and *T. cruzi*. However, ATP citrate lyase and synthase are absent from all trypanosomatids including *Paratrypanosoma*, implying that they are unable to convert mitochondrial acetyl-CoA to citrate. Only *Paratrypanosoma* and Leishmaniinae are able to convert and subsequently oxidize methionine into succinyl-CoA. Finally, the tryptophan degradation pathway is present in *N. gruberi*, *T. borreli*, *B. saltans*, as well as *Paratrypanosoma*, but lost from all other trypanosomatids (Dataset S10).

Discussion

We have demonstrated that *Paratrypanosoma*, the most basal-branching trypanosomatid derived from free-living bodonids (2), assumes three different morphotypes characteristic of trypanosomatids. In a liquid cultivation medium, it alternates between motile promastigote and surface-attached haptomonad morphologies, both capable of division. Transfer to an agar plate triggers transformation into another distinct morphotype: an amastigote. As these morphotypes are common among mono- and dixenous trypanosomatids, this indicates that the ancestral trypanosomatid likely had morphological flexibility, advantageous when faced with dramatically different conditions during the evolution of parasitism of invertebrate and vertebrate hosts. Therefore, the trait of extensive interstage morphological transformation of *Leishmania* and *Trypanosoma* in their mammalian and insect hosts likely existed in their monoxenous predecessor; the wide array of trypanosomatid morphotypes (10) did not originate within the context of dixenous parasitism but predated the two-host lifestyle (25).

The capacity to firmly but transiently attach to a substrate by the flagellum, apparently preventing their discharge from the host, is common in trypanosomatids. Bodonids can also undergo surface attachment (24). This feature might have predisposed trypanosomatids for their initial radiation in insects (1), which required fixation to the host gut. Attachment associated with extensive remodeling of the flagellum, as in other trypanosomatids (22), seems to be a central feature in the life cycle of *Paratrypanosoma*. Attachment and flagellum shortening could occur without a division event, while we only observed flagellum growth and detachment following division of a haptomonad. This has similarities to both *Leishmania*, in which flagellum shortening can occur without division, and *T. brucei*, in which division to generate dissimilar daughters is used for life cycle stage transition. Remodeling of the flagellum in haptomonads involved expansion of flagellum/cell attachment in the distal pocket region, suggesting the FAZ proteins may contribute to surface attachment.

OG gains and losses indicate *Paratrypanosoma* has diverged significantly from the common ancestor of trypanosomatids (Fig. S6), however it has retained more ancestral OGs than any trypanosomatid lineages except stercorarian trypanosomes (Fig. 3). Recent comparison of the *B. saltans* and trypanosomatid genomes revealed that metabolic losses accompanied the emergence of obligatory parasitism (3) with little further gene loss or streamlining
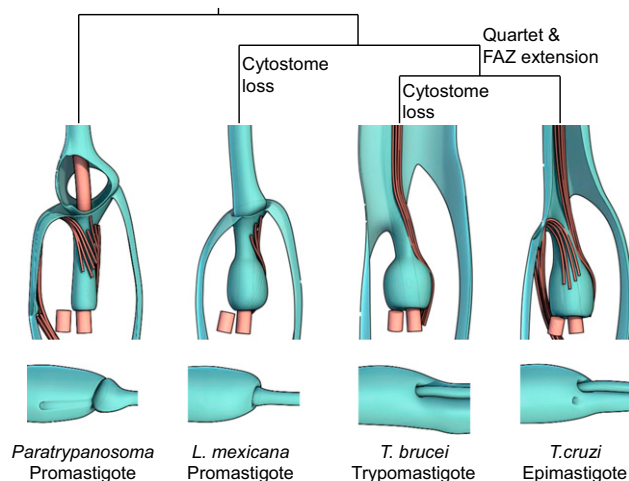

Fig. 6. Evolution of the flagellar pocket/cytostome complex of human infective trypanosomatids. Cartoon summarizes the likely loss of the cytostome and extension of the microtubule quartet and FAZ to generate *Leishmania*, *T. brucei*, and *T. cruzi* pocket/cytostome morphology from an ancestral *Paratrypanosoma*-like morphology.

MEDICAL SCIENCES

of the genome occurring later (4, 25). Indeed, our analyses revealed a massive loss of proteases, peptidases, and cathepsins involved in the breakdown of polypeptides. *Paratrypanosoma* and other trypanosomatids have also lost receptor-mediated endocytosis of macromolecules, cobalamin biosynthesis, and lysosomal pro-X exopeptidase and ammonium transporter, compelling trypanosomatids into foraging nitrogen from other sources. *Paratrypanosoma* has gained or expanded several gene families that were not present in its free-living predecessor, including transmembrane transporters suitable for scavenging amino acids and other metabolites from the host (3, 4, 18). An interesting gene family expansion, which likely occurred early in the evolution of trypanosomatids, are the DGF1 genes, present in *Paratrypanosoma* and the stercorarian trypanosomes only. These abundant secreted proteins may play a role in host–parasite interactions (21, 22).

The ultrastructure of *Paratrypanosoma* includes a *Leishmania*-like FAZ including a microtubule quartet and a *T. cruzi*-like cytostome. This supports the hypothesis that the extended FAZ evolved once in the *Trypanosoma* lineage and indicates that the cytostome was an ancestral feature, retained in *T. cruzi* but lost in *T. brucei*, *Leishmania*, *Phytomonas*, and several monoxenous lineages (Fig. 6). This implies that there has been a streamlining of ultrastructure analogous to the streamlining of the genome, with the notable exception of innovation to generate an extended FAZ in *Trypanosoma*.

The differences in transcriptome of *Paratrypanosoma* promastigotes and haptomonads coexisting in culture are comparable in magnitude to the differences between *L. mexicana* amastigotes (mammalian host) and promastigotes (sandfly vectors) (18, 23).

Our analysis of the morphologies *Paratrypanosoma* can attain in culture, its genome and transcription profile, and the ultrastructure of the flagellar pocket/cytostome complex has uncovered features likely present in the ancestors of the three human-infective trypanosomatid lineages (Fig. 6). Future studies of this very interesting protist will be particularly informative in regard to how trypanosomatid parasites have evolved from the free-living bodonids.

Materials and Methods

Promastigotes and haptomonads were cultured at 27 °C in a 1:1 mixture of RPMI 1640 and M199, pH 7.0, with 10% (vol/vol) FCS, 2% sterile human urine, 10 μg/mL hemin, and penicillin–streptomycin, and interconversion was analyzed by time-lapse microscopy in culture. Amastigotes were generated by culture on agarose plates. For SEM, haptomonads were grown and fixed on coverslips. For TEM, they were grown in culture flasks, treated with propylene–oxide treatment to dissolve the substrate, and then prepared by high-pressure freezing. Detailed culture and EM methods, genome assembly and annotation, transcriptome analysis, and gene family/ontology methods are available in *SI Materials and Methods*.

1. Maslov DA, Votýpka J, Yurchenko V, Lukeš J (2013) Diversity and phylogeny of insect trypanosomatids: All that is hidden shall be revealed. *Trends Parasitol* 29:43–52.
2. Flegontov P, et al. (2013) *Paratrypanosoma* is a novel early-branching trypanosomatid. *Curr Biol* 23:1787–1793.
3. Opperdoes FR, Butenko A, Flegontov P, Yurchenko V, Lukeš J (2016) Comparative metabolism of free-living *Bodo saltans* and parasitic trypanosomatids. *J Eukaryot Microbiol* 63:657–678.
4. Jackson AP, et al. (2016) Kinetoplastid phylogenomics reveals the evolutionary innovations associated with the origins of parasitism. *Curr Biol* 26:161–172.
5. Ginger ML, Portman N, McKean PG (2008) Swimming with protists: Perception, motility and flagellum assembly. *Nat Rev Microbiol* 6:838–850.
6. Wheeler RJ, Gluenz E, Gull K (2015) Basal body multipotency and axonemal remodelling are two pathways to a 9+0 flagellum. *Nat Commun* 6:8964.
7. Langousis G, Hill KL (2014) Motility and more: The flagellum of *Trypanosoma brucei*. *Nat Rev Microbiol* 12:505–518.
8. Szempruch AJ, et al. (2016) Extracellular vesicles from *Trypanosoma brucei* mediate virulence factor transfer and cause host anemia. *Cell* 164:246–257.
9. Imhof S, et al. (2016) Flagellar membrane fusion and protein exchange in trypanosomes; a new form of cell-cell communication? *F1000Res* 5:682.
10. Wheeler RJ, Gluenz E, Gull K (2013) The limits on trypanosomatid morphological diversity. *PLoS One* 8:e79581.
11. Wheeler RJ, Sunter JD, Gull K (2016) Flagellar pocket restructuring through the *Leishmania* life cycle involves a discrete flagellum attachment zone. *J Cell Sci* 129:854–867.
12. Alcantara CL, Vidal JC, de Souza W, Cunha-e-Silva NL (2014) The three-dimensional structure of the cytostome-cytopharynx complex of *Trypanosoma cruzi* epimastigotes. *J Cell Sci* 127:2227–2237.
13. Beattie P, Gull K (1997) Cytoskeletal architecture and components involved in the attachment of *Trypanosoma congolense* epimastigotes. *Parasitology* 115:47–55.
14. Vickerman K, Tetley L (1990) Flagellar surfaces of parasitic protozoa and their role in attachment. *Ciliary and Flagellar Membranes*, ed Bloodgood RA (Booknews, London), pp 267–304.
15. Wakid MH, Bates PA (2004) Flagellar attachment of *Leishmania* promastigotes to plastic film *in vitro*. *Exp Parasitol* 106:173–178.
16. Killick-Kendrick R, Molyneux DH, Ashford RW (1974) *Leishmania* in phlebotomid sandflies. I. Modifications of the flagellum associated with attachment to the mid-gut and oesophageal valve of the sandfly. *Proc R Soc Lond B Biol Sci* 187:409–419.
17. del Pilar Corena M, et al. (2005) Carbonic anhydrase in the adult mosquito midgut. *J Exp Biol* 208:3263–3273.
18. Flegontov P, et al. (2016) Genome of *Leptomonas pyrrhocoris*: A high-quality reference for monoxenous trypanosomatids and new insights into evolution of *Leishmania*. *Sci Rep* 6:23704.
19. Simão FA, Waterhouse RM, Ioannidis P, Kriventseva EV, Zdobnov EM (2015) BUSCO: Assessing genome assembly and annotation completeness with single-copy orthologs. *Bioinformatics* 31:3210–3212.
20. Emms DM, Kelly S (2015) OrthoFinder: Solving fundamental biases in whole genome comparisons dramatically improves orthogroup inference accuracy. *Genome Biol* 16:157.
21. Lander N, et al. (2010) Localization and developmental regulation of a dispersed gene family 1 protein in *Trypanosoma cruzi*. *Infect Immun* 78:231–240.
22. Lacomble S, Portman N, Gull K (2009) A protein-protein interaction map of the *Trypanosoma brucei* paraflagellar rod. *PLoS One* 4:e7685.
23. Fiebig M, Kelly S, Gluenz E (2015) Comparative life cycle transcriptomics revises *Leishmania mexicana* genome annotation and links a chromosome duplication with parasitism of vertebrates. *PLoS Pathog* 11:e1005186.
24. Brooker BE (1971) Fine structure of *Bodo saltans* and *Bodo caudatus* (Zoomastigophora: Protozoa) and their affinities with the Trypanosomatidae. *Bull Br Mus Nat Hist* 22:89–102.
25. Janouškovec J, Keeling PJ (2016) Evolution: Causality and the origin of parasitism. *Curr Biol* 26:R174–R177.

Supporting Information

Skalický et al. 10.1073/pnas.1712311114

SI Materials and Methods

***Paratrypanosoma* Cultivation and Sample Preparation for Electron Microscopy.** The axenic culture was maintained at 27 °C in a mix of RPMI 1640 and M199 cultivation media (1:1) at pH 7.0 with addition of 10% (vol/vol) FCS, 2% sterile human urine, 10 μg/mL of hemin, and penicillin–streptomycin. Amastigotes were generated by culture on semisolid agarose plates. Autoclaved 3% [wt/vol] agarose was cooled to 65 °C and diluted 10 times in a prewarmed cultivation medium. The resulting 0.3% agarose solution was poured into Petri dishes (85 × 15 mm), dried for 1 h in a laminar flow hood, and inoculated with $4 × 10^5$ or $2 × 10^6$ resuspended log-phase cells. Light and electron microscopy (EM) were performed as described previously (2). For scanning EM, haptomonads were grown and fixed directly on coverslips, while for high-pressure freezing transmission EM (2), they were prepared using propylene–oxide treatment to dissolve the plastic substrate as described elsewhere (15). Electron tomography was performed as described previously (8).

Time-Lapse Videos. Promastigote/haptomonad interconversion was analyzed by automated time-lapse videomicroscopy. Log phase ($1 × 10^6$ cells per mL) promastigote culture was transferred into a 35-mm μ-dish with a glass bottom (iBidi) and recorded for 24 h at 20 °C in a chamber with controlled temperature.

Experimental Infection of Mosquitoes and Mice. Two different ways of infecting laboratory-reared mosquitoes (*C. quinquefasciatus*) were tested. Mosquitoes were starved for 24 h and then fed for 2 h on a cotton pellet presoaked in a 10% sugar solution with *Paratrypanosoma*, which was shown to survive in this solution for up to 2 d. Two independent experiments each with 50 mosquitoes were performed with 10^6 and 10^7 late log cells. Forty mosquito females were infected also by feeding through a chick-skin membrane on suspension of parasites mixed 1:10 with heat-inactivated rabbit blood (final concentration was 10^7 late log cells per mL). Engorged mosquitoes were separated and maintained in the appropriate conditions (23 °C, 80% humidity, 12 h day/light). The presence of *Paratrypanosoma* in mosquito intestine was checked on days 1, 2, 3, 4, 6, and 14 postinfection by dissection of 4–10 specimens at each time point. Four laboratory BALB/c mice were intraperitoneally and s.c. injected with 10^7 late log stage cells. The course of infection was recorded weekly for 1 mo (the mice were bled from the tail).

Attachment Plaque Digestion. To assess attachment plaque resistance to digestive enzymes, haptomonad culture was incubated with various enzymes for 3 h with regular intense shaking (Dataset S1), and detached cells were counted. For immunofluorescence, $1 × 10^7$ pelleted cells were fixed for 10 min with 4% (wt/vol) para-formaldehyde in phosphate-buffered solution (PBS), rinsed in PBS, allowed to settle on a poly-L-lysine–coated slide, kept for 1 h in a blocking buffer containing 5% [wt/vol] nonfat dry milk in PBS, and for 2 h incubated with one of the following primary antibodies: anti-PFR2 (24) or anti-DOT1. After their removal, the cells were incubated for 1 h in blocking buffer with Alexa Fluor 488-conjugated secondary antibody, rinsed with PBS, mounted in DAPI-containing ProLong diamond antifade reagent, and observed.

Genome and Transcriptome Assembly and Annotation. Genome assembly was made with GS De Novo Assembler (Newbler) v2.9 using reads obtained on the Illumina MiSeq platform combining 3.4 million reads from a paired-end library (insert size, 0.4 kb;

average read length upon trimming, 241 nt; 29× coverage) and 4 million reads from a mate-pair library (insert size, 1–8 kb; average read length upon trimming, 255 nt; 34× coverage). Total RNA and poly(A)-enriched fractions were used to prepare MiSeq paired-end libraries (insert size, 0.28 kb; read length, 150 nt) to sequence the transcriptome with the Illumina MiSeq system, resulting in 34 and 37 million high-quality reads, respectively. All sequencing data were deposited to the TriTrypDB (tritrypdb.org/tritrypdb/). Transcriptomic reads were aligned to the genome assembly using Bowtie2 v. 2.2.5 with the "–end-to-end" and "–very-sensitive" options. Augustus v2.5.5 was used for annotation, and its accuracy was improved by retraining with a set of 100 highly conserved gene models. The annotation was further manually enhanced as follows: Transcribed ORFs longer than 100 amino acids, not predicted by Augustus, were added to the annotation, and gene models with start sites predicted in regions with no transcription were corrected based on RNA-seq data. Subsequently, Blast2GO programs were used to obtain functional gene annotations. To analyze differential gene expression, three independent replicates of transcriptomic Illumina HiSeq libraries from both sessilemastigotes and promastigotes were generated. Differential gene expression analysis of six libraries with ~50 million reads each (insert size, 280 bp; read length, 101 nt) was performed using a procedure described elsewhere (19).

Gene Family, Gene Ontology, and Differential Expression Analyses. OGs were inferred using Orthofinder software v.0.61 (21). Annotated proteins of 29 kinetoplastid species and a heterolobosean outgroup (Dataset S2) downloaded from TriTrypDB v. 31, Marine Microbial Eukaryote Transcriptome Sequencing Project (marinemicroeukaryotes.org/), and Welcome Trust Sanger Institute (www.sanger.ac.uk/resources/downloads/protozoa/) were combined with newly annotated proteins of *Paratrypanosoma* and *Blechomonas ayalai*. The Count program was subsequently used for mapping gene family gains/losses (the Dollo parsimony algorithm) onto a reference species cladogram based on a multigene phylogenetic tree. Each protein, from a set of 98 unique proteins present in all species, was separately aligned using mafft, and informative positions with consecutive concatenation was performed using Gblocks. A multiprotein tree was constructed using RAxML v. 8.2.1 (LG+Γ model) with 1,000 bootstraps and Phylobayes v. 4.1c (GTR+Γ+CAT model) running eight independent chains for 10,000 cycles.

Gene ontology (GO) annotation of *Paratrypanosoma* gene families gained or lost at selected nodes was performed using the Blast2GO software with the following settings: BLASTP (10^{-10} E-value cutoff) was run using Blast2GO's CloudBlast service, retaining the best 20 hits and filtering low-complexity regions. Mapping GO terms onto Blast hits was followed by selection of the most specific GO terms (an annotation cutoff of 55 was used). Resulting annotations were visualized by generation of GO graphs and multilevel pie charts for each GO term category (cellular component, biological process, and molecular function). A differential expression analysis using transcriptomic data from both promastigotes and haptomonads was conducted in CLC Genomic Workbench v8, and only genes with an expression fold-change ≥ 2 and an FDR-corrected P value ≤ 0.05 were analyzed further. GO term enrichment was also analyzed for protein-coding genes significantly over/underexpressed in haptomonads compared with promastigotes, versus all protein-coding genes using Fisher's exact test with a FDR corrected P value cutoff of 0.05.

Fig. S1. Cartoon of the attachment process. (*A*) Frames from time-lapse video of promastigote and haptomonad interconversion. (Magnification: 100×.) (*B*) Cartoon depicting this process. The promastigote freely swims and can attach to a surface by the bulge. The flagellum shortens and the cell assumes an upright position with the bulge expanding into a thin attachment pad. Division events can generate cells that either attach to the surface or grow a long flagellum and leave the colony.
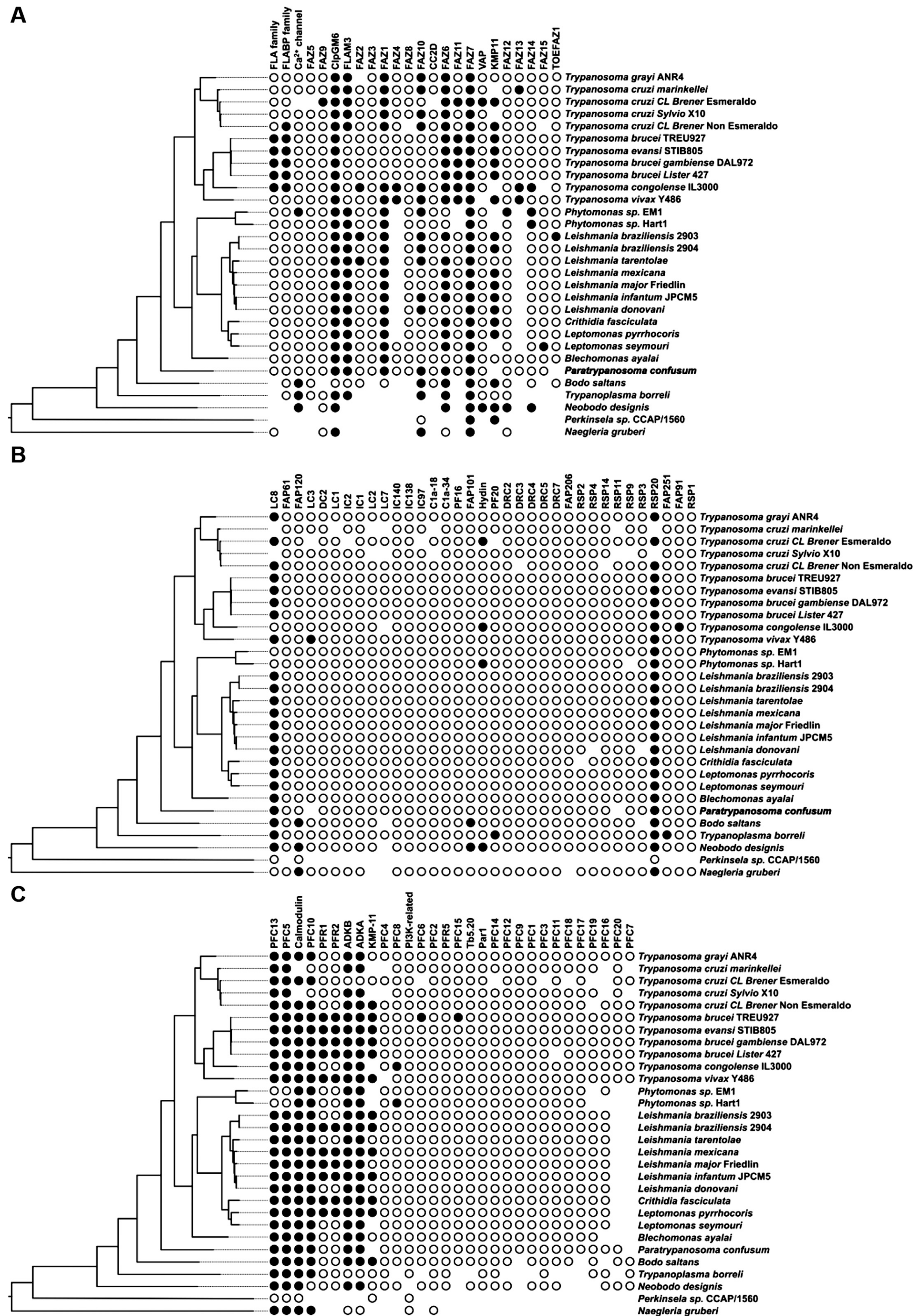
Fig. S2. Conservation of cytoskeletal proteins across the trypanosomatids. Matrix summarizing the presence of a single (open circle), multiple (filled circle), or no (space) orthologs of a gene family for (A) FAZ, (B) axoneme, and (C) PFR genes.
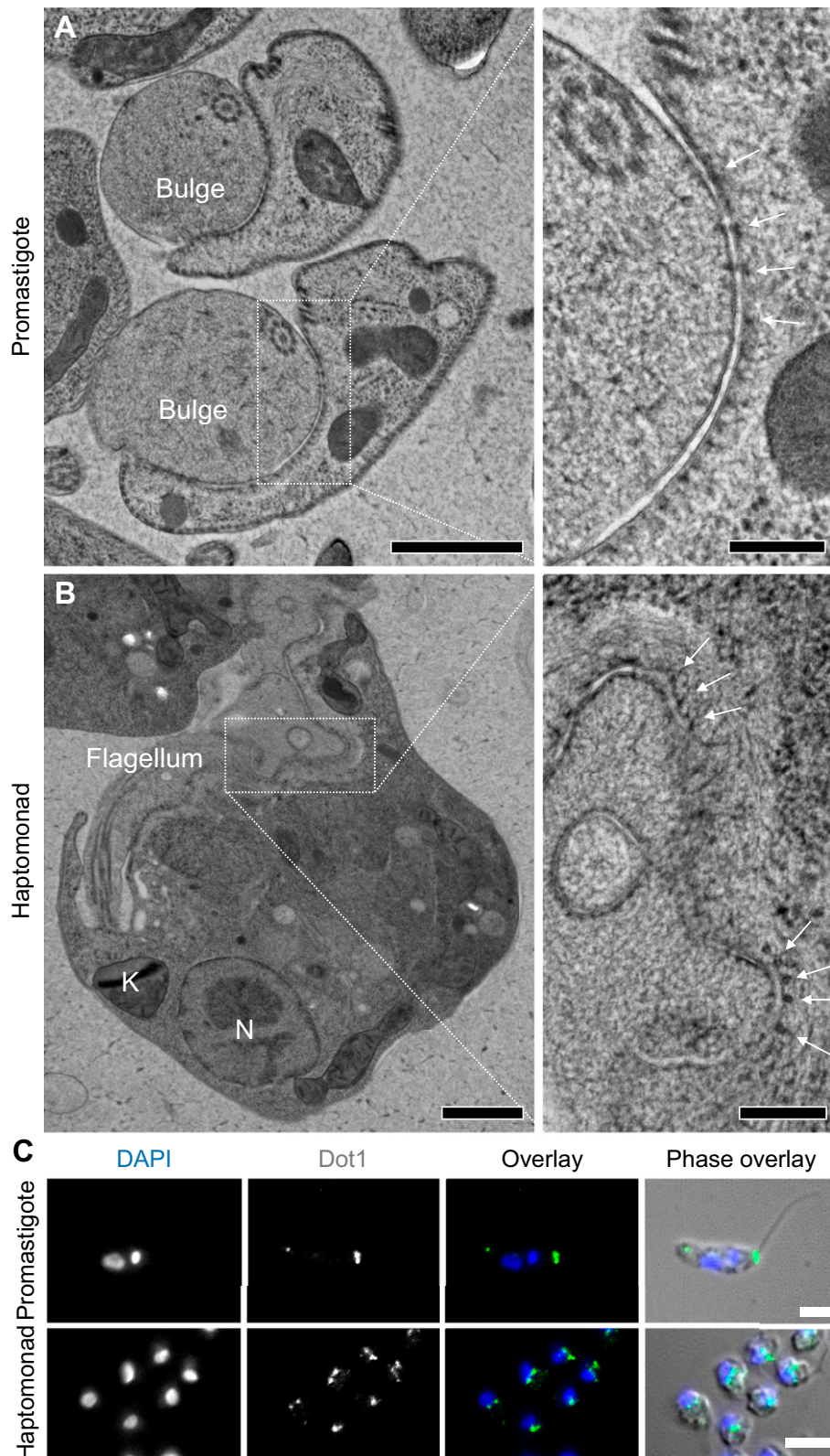
Fig. S3. The flagellar bulge is elaborated in haptomonads for surface attachment. (*A*) Detail of attachment between the flagellum/bulge with the cell body in the promastigote. (*B*) Detail of attachment between the flagellum/bulge with the haptomonad cell body. (*C*) Immunofluorescence using Dot1, a *T. brucei* anti-FAZ antibody, of promastigotes and haptomonads. Dot1 labels a distal ring or horseshoe structure in promastigotes, similar to the localization of FAZ10 in *Leishmania*. The localization is elaborated in haptomonads. Desmosome-like attachments, similar to the *T. brucei* and *Leishmania* FAZ, are indicated with arrows. [Scale bars, (*A*) 1 μm, detail 250 nm; (*B*) 1 μm, detail 250 nm; (*C*) 2 μm.] K, kinetoplast; N, nucleus.

Fig. S4. *Paratrypanosoma* has a cytostome similar to *T. cruzi* and a pocket architecture similar to *Leishmania*. (*A*) SEM of the promastigote showing an indentation, similar to an extended *T. cruzi* preoral ridge, extending from the flagellar pocket to the cytostome. (*B*) Cartoon of the pocket/cytostome of *Paratrypanosoma*, based on TEM of the flagellar pocket. A set of highly decorated microtubules runs from inside the pocket (15) around the end of the flagellar pocket neck (8) to the cell pellicle and back to the cytostome. [Scale bars, (*A*) 5 μm, detail is 3.3 times enlarged, (*B*, *1*, *2*, and *4*) 250 nm, and (*B* and *3*) 500 nm.]

Fig. S5. Restructuring of the *Paratrypanosoma* flagellum between promastigotes, haptomonads, and amastigotes. Shown is the TEM of longitudinal sections through the flagellar pocket and transverse sections through the protruding portion of the flagellum in the promastigote, haptomonad, and amastigote. Ninefold Markham rotational averaging of axoneme structure shows the presence of inner and outer dynein arms and radial spokes in the amastigote, promastigote, and haptomonad. White arrows indicate the basal plate. (Scale bar, 500 nm and flagellar details 200 nm.)
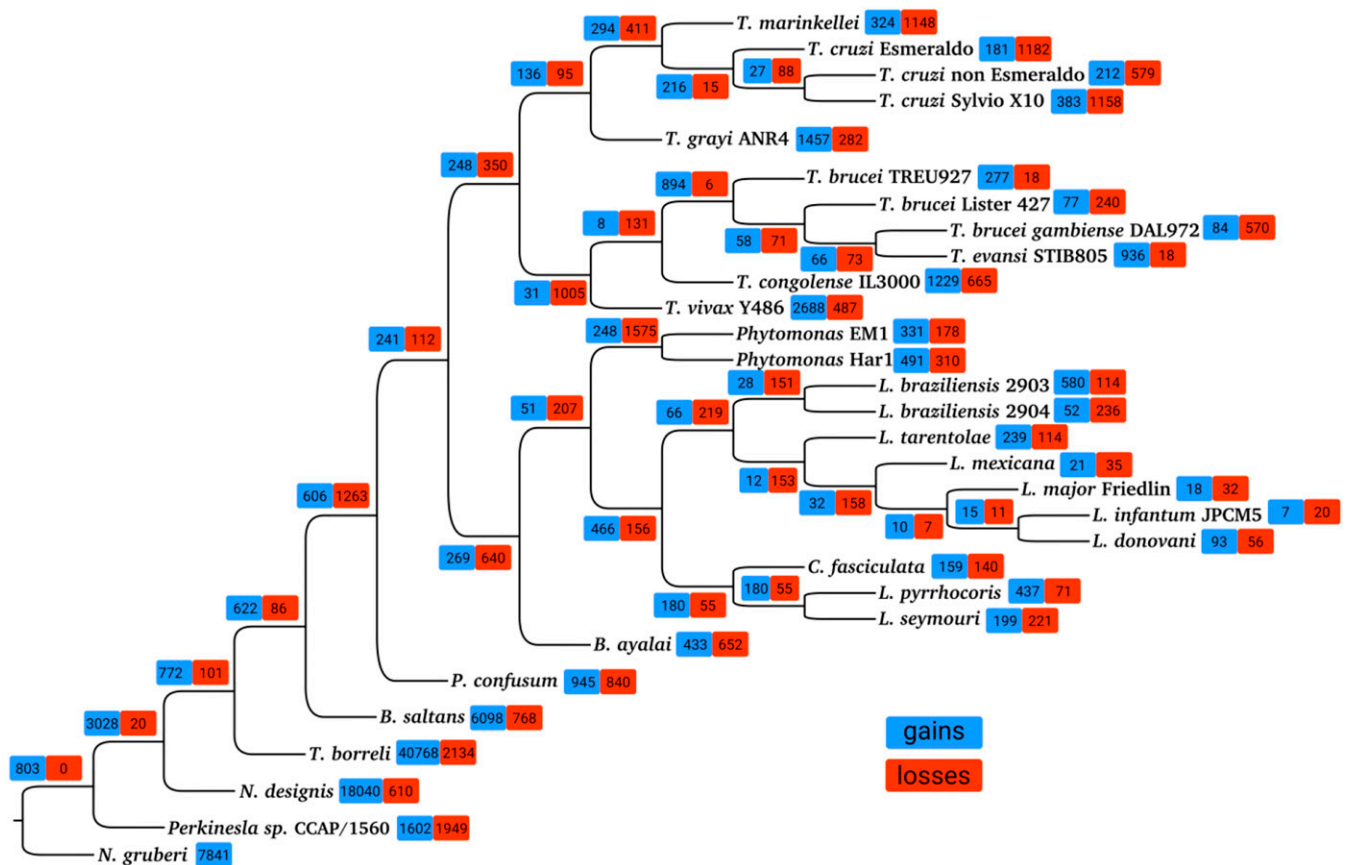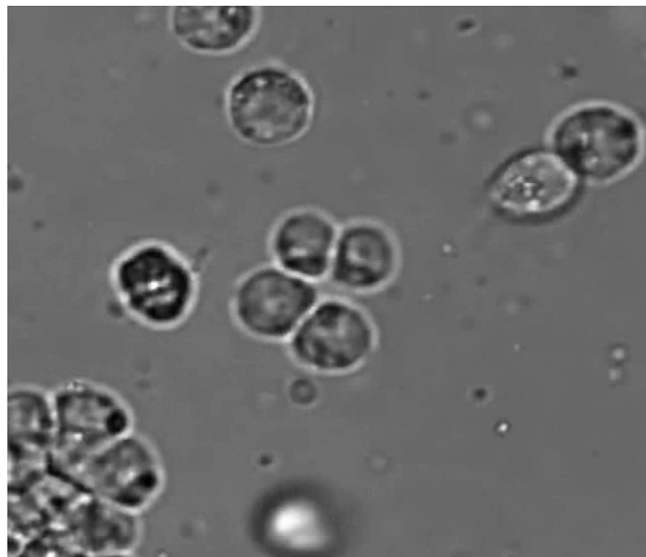
Fig. S6. Gene family gains/losses mapped on cladogram using Dollo parsimony. Gained and lost gene families (GOs) are mapped on the cladogram, the topology of which was obtained from multiprotein phylogenetic analysis. Gene families gained are labeled in blue, and gene families that were lost are in red.

Movie S1. Time-lapse video showing promastigote-to-haptomonad transformation, multiple divisions, and recreation of motile promastigote cells after division. Video shows time span of about 5 h and 30 min of real time.

Movie S1
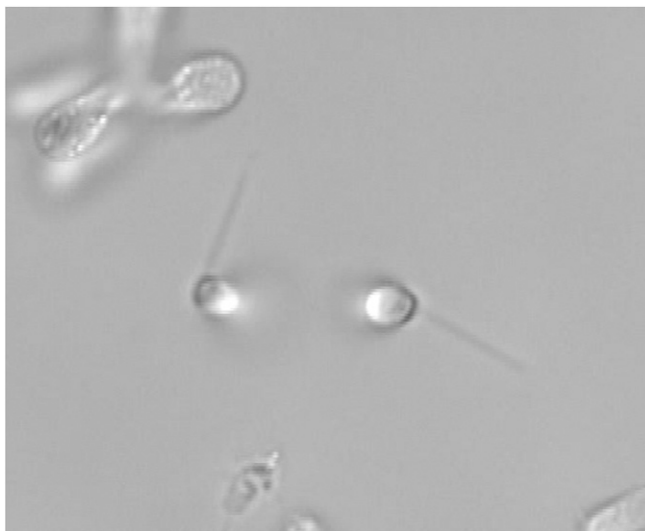
Movie S2. Time-lapse video showing promastigote-to-haptomonad transformation, with a focus on cell flagellum and cell division. Video shows time span of about 5 h of real time.

[Movie S2](#)

Dataset S1.   List of enzymes

[Dataset S1](#)

(*A*) List of enzymes used to digest the attachment pad of haptomonads kept for 24 h in the cultivation medium. Enzymes are listed according to their activity. For some enzymes (marked with an asterisk), the concentration is listed in units. (*B*) List of enzymes used to digest the attachment pad of haptomonads kept for 3 h in 1× PBS. Enzymes are listed according to their activity.

Dataset S2.   Phyletic patterns, differential expression data, and annotations for all *Paratrypanosoma* genes

[Dataset S2](#)

Expression measured in RPKM at both life cycle stages, fold-change, and FDR-corrected *P* value are shown for each gene.

Dataset S3.   GO terms significantly enriched in gene sets up-regulated in haptomonads and promastigotes

[Dataset S3](#)

(*A*) GO terms significantly enriched (FDR-corrected *P* value < 0.05) in haptomonads. (*B*) GO terms significantly enriched in promastigotes.

Dataset S4.   Genomes used for gene family analyses

[Dataset S4](#)

Genomes were obtained from publicly available databases such as Welcome Trust, GenBank, TriTrypDB (version 31), or Marine Microbial Eukaryote Transcriptome Sequencing Project (MMETSP).

Dataset S5.   Annotations of ancestral genes retained in *Paratrypanosoma* and lost in the other trypanosomatids

[Dataset S5](#)

Paratrypanosoma genes belonging to OGs with this phyletic pattern are shown. Annotations were generated using Blast2GO. Metabolic proteins are highlighted.

Dataset S6. Annotations of ancestral genes retained in *Paratrypanosoma* and lost in the other trypanosomatids

Dataset S6

Paratrypanosoma genes belonging to OGs with this phyletic pattern are shown. Annotations were generated using Blast2GO. Metabolic proteins are highlighted as well as proteins of the DGF.

Dataset S7. Relationship of phyletic patterns and stage-specific gene expression in *Paratrypanosoma*

Dataset S7

One-way ANOVA analysis combined with Tukey's honest significance test shows that differential gene expression at the haptomonad and promastigote stages depends on phyletic patterns of corresponding OGs (P value = 1.22×10^{-7}). The presence/absence patterns across six species groups (phyletic patterns) are shown in the leftmost rows and on top of the matrix. Genes were grouped by phyletic patterns, and for each group, average fold-change was calculated. Positive fold-change corresponds to up-regulation in haptomonads, and negative fold-change to up-regulation in promastigotes. Number of genes with significant stage-specific differences in expression is also shown for each group. ANOVA P values corrected for multiple testing appear in each cell of the matrix and represent pairwise comparisons of gene groups.

Dataset S8. Genes belonging to OGs gained at the *Trypanosoma* node

Dataset S8

Genes gained at the *Trypanosoma* node were identified by Count program, applying Dollo parsimony analysis on the OGs created by Orthofinder. Appropriate proteins were extracted from a working dataset of proteoms and blasted in Blast2GO against nr protein database with default settings. Column labels describe to which OG proteins belong, their gene ID, description, protein length, number of blast hits, E-value, and average % similarity.

Dataset S9. Differential expression of cytoskeletal proteins in haptomonads and promastigotes

Dataset S9

Genes significantly up-regulated in haptomonads (Dataset S2) are marked in green color. Multigene families are also highlighted with various colors.

Dataset S10. Presence/absence of selected metabolic enzymes in all analyzed species

Dataset S10

Presence is marked with green color and absence in red, respectively. Numbers represent number of gene copies in each species. Abbreviations: Baya, *B. ayalai*; Bsal, *B. saltans*; Cfas, *C. fasciculate*; Lbr1, *Leishmania braziliensis* MHOM/BR/75/M2903; Lbr2, *L. braziliensis* MHOM/BR/75/M2904; Ldon, *Leishmania donovani*; Linf, *Leishmania infantum*; Lmaj, *L. major* Friedlin; Lmex, *L. mexicana*; Ltar, *Leishmania tarentolae*; Lpyr, *L. pyrrhocoris*; Lsey, *Leptomonas seymouri*; Ndesig, *N. designis*; Ngrub, *N. gruberi*; Pconf, *P. confusum*; Pem1, *Phytomonas* sp. EM1; Perk, *Perkinsela* sp. CCAP-1560; Phar, *Phytomonas* sp. HART1; Tbor, *T. borreli*; Tbr1, *T. brucei* Lister 427; Tbrg, *T. brucei gambiense* DAL972; Tbru, *T. brucei* TREU927; Tcon, *Trypanosoma congolense*; Tcr1, *T. cruzi* CL Brener Esmeraldo-like; Tcr2, *T. cruzi* CL Brener Non-Esmeraldo-like; Tcr5, *T. cruzi* Sylvio; Teva, *Trypanosoma evansi*; Tgra, *T. grayi*; Tmar, *T. cruzi marinkellei*; Tviv, *Trypanosoma vivax*.